HHS Public Access

Author manuscript

Small. Author manuscript; available in PMC 2025 November 01.

Published in final edited form as:

Small. 2024 November ; 20(48): e2403560. doi:10.1002/smll.202403560.

Liver-on-a-Chip Integrated with Label-free Optical Biosensors for Rapid and Continuous Monitoring of Drug-induced Toxicity

Jia-Wei Yang[+],
Terasaki Institute for Biomedical Innovation, 21100 Erwin St, Woodland Hills, CA 91367, USA

Danial Khorsandi[+],
Terasaki Institute for Biomedical Innovation, 21100 Erwin St, Woodland Hills, CA 91367, USA

Luis Trabucco,
The University of Texas at San Antonio, Department of Biomedical Engineering and Chemical Engineering, One UTSA Circle, San Antonio, TX, 78249, USA

Maisha Ahmed,
The University of Texas at San Antonio, Department of Biomedical Engineering and Chemical Engineering, One UTSA Circle, San Antonio, TX, 78249, USA

Ali Khademhosseini,
Terasaki Institute for Biomedical Innovation, 21100 Erwin St, Woodland Hills, CA 91367, USA

Mehmet Remzi Dokmeci[*],
Terasaki Institute for Biomedical Innovation, 21100 Erwin St, Woodland Hills, CA 91367, USA

Jing Yong Ye[*],
The University of Texas at San Antonio, Department of Biomedical Engineering and Chemical Engineering, One UTSA Circle, San Antonio, TX, 78249, USA

Vadim Jucaud[*]
Terasaki Institute for Biomedical Innovation, 21100 Erwin St, Woodland Hills, CA 91367, USA

Abstract

Drug toxicity assays using conventional two-dimensional static cultures and animal studies have limitations preventing the translation of potential drugs to the clinic. The recent development of organs-on-a-chip platforms provides promising alternatives for drug toxicity/screening assays. However, most studies conducted with these platforms only utilize single endpoint results, which do not provide real-time/ near real-time information. Here, we present a versatile technology that integrates a three-dimensional liver-on-a-chip with a label-free photonic crystal-total internal reflection (PC-TIR) biosensor for rapid and continuous monitoring of the status of cells. This technology can detect drug-induced liver toxicity by continuously monitoring the secretion rates and levels of albumin (for assessing liver function) and glutathione S-transferase α (GST-α) (for assessing injury) of a 3D liver on-a-chip model treated with Doxorubicin, a chemotherapeutic drug. The PC-TIR biosensor is based on a one-step antibody functionalization with high

[*]Corresponding authors: mdokmeci@terasaki.org; jingyong.ye@utsa.edu; and vjucaud@terasaki.org.
[+]These authors equally contributed to this work.

specificity and a detection range of 21.68 ng/mL to 7834.30 ng/mL for albumin and 2.198 ng/mL to 794.33 ng/mL for GST-α. This approach provides critical advantages for the early detection of drug toxicity and improved temporal resolution to capture transient drug effects. The proposed proof-of-concept study introduces a scalable and efficient plug-in solution for organ-on-a-chip technologies, advancing drug development and *in vitro* testing methods by enabling timely and accurate toxicity assessments.

Graphical Abstract

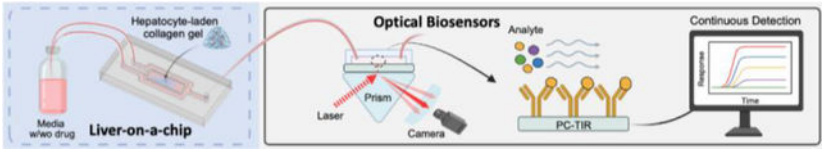

This study presents a liver-on-a-chip platform integrated with an optical sensor for rapid and continuous monitoring of drug-induced toxicity. It accurately detects albumin and GST-α levels, providing ongoing data on liver function and injury. This technology advances drug development by enabling timely and precise toxicity assessments.

Keywords

liver-on-a-chip; drug toxicity; optical biosensor; rapid detection; continuous detection

1. Introduction

Organ-on-a-chip (OoC) technology is emerging as a powerful platform for drug screening, toxicity, and many other studies potentially replacing animal testing in the long run [1]. This technology provides an analog of human tissue functions *in vitro* [2], opening new doors for many studies, including drug screening [3, 4], cancer metastasis [5, 6], pharmacokinetics, and pharmacodynamics [7, 8]. These OoC models could reproduce important human physiological functions and show significant potential in preclinical testing [9, 10]. A recently developed liver-on-a-chip model demonstrated 87% sensitivity and 100% specificity in drug toxicity testing, effectively identifying drugs that passed preclinical toxicology tests in animals but induced liver toxicity in clinical trials [11]. However, current studies using OoC technology mainly rely on single endpoint measurements to evaluate the outcome of experiments, including the status of cells and physiological markers [12], yet none have a real-time/ near real-time understanding of the status of the cells. It is noted in recently published studies that rapid and continuous monitoring is crucial for capturing dynamic processes like drug-induced liver injury, which cannot be accurately characterized using only endpoint measurements [13]. Therefore, having a microfluidics amenable monitoring system integrated with an OoC model that supports rapid and continuous monitoring would provide unprecedented insights into understanding transient drug responses and cumulative toxicity effects to improve drug development and streamline preclinical pharmacological evaluation [14].

Integrating in-line biosensors with OoC enables *in situ* and rapid, continuous monitoring of tissue characteristics and functions. This advancement represents a paradigm shift by offering significant advantages over conventional endpoint fluorescent imaging/probes and molecular biology analysis techniques. In particular, in-line biosensors are minimally invasive and allow for the continual monitoring of OoC. State-of-the-art sensors that measure parameters such as temperature, O_2/CO_2 levels, pH, and transepithelial electrical resistance have been utilized in various OoC platforms [15]. These *in situ* monitoring strategies provide critical information about the microenvironment, biological properties, and status of cells and tissues within the OoC. While there have been advances in detecting specific cell-secreted biomarkers, including lactate, IL-6, and GST-α, most of these analytical methods rely primarily on electrochemical (EC) biosensors [15]. Current EC biosensors typically measure specific biomarkers at intervals of several minutes to hours, preventing proper real-time dynamic monitoring. Since many drug-induced cellular responses are dynamic, there is a strong need for biosensing technologies with increased temporal resolution to capture and study transient drug-induced toxicity effectively.

Optical biosensors based on surface plasmon resonance (SPR) provide a label-free bioassay platform for the real-time quantitative detection of various biomolecules, such as antibodies, proteins, enzymes, and nucleic acids [16–18]. SPR biosensors are a label-free technology that provides time-dependent direct detection of specific analyte association/dissociation kinetics. The measurement principle of SPR biosensors is based on monitoring changes in the refractive index of the biosensor surface induced by binding events. These changes in the refractive index indicate molecular interactions and are measured in real time without the need for labels, providing a direct correlation to the mass concentration of the target analyte present in the sample. However, few SPR platforms have been successful in cell culture monitoring, primarily due to the complexity of the culture medium and the associated mass transfer issues [19]. These challenges can lead to signal interference and inaccurate measurements [20]. Moreover, using labeled detection methods, such as fluorescent or luminescent tags, introduces complexities and potential interferences, including photobleaching, quenching, and nonspecific binding. These methods often have limited detection ranges and can interfere with the biological processes being studied. Additionally, labeled methods require more time for preparation and processing, which can delay the acquisition of results and reduce the efficiency of rapid and continuous monitoring [21, 22].

Photonic crystal-total internal reflection (PC-TIR) biosensors have been used to detect biomarkers in a label-free manner. The sensor is based on a unique open optical microcavity formed between a piece of 1-dimensional (1D) PC structure and a TIR interface. The 1D PC structure consists of multilayers of dielectric coatings, which can be easily and cost-effectively fabricated using well-established vacuum deposition techniques. Compared to EC sensors, optical sensors do not require wires or electrical connections, simplifying the detection process. The unique open optical microcavity of the PC-TIR sensor offers a smooth biosensing surface for easy access to analyte molecules. It has a sharp resonance spectral width (~1–2 nm) for sensitive and accurate bioassays and a robust sensing surface composed of dielectric materials for potentially long-term and continuous monitoring of cell secretome.

Here, we present the first integration of an organ-on-a-chip system with a PC-TIR biosensor (Figure 1). This integration allows for continuous, label-free monitoring of secreted biomarkers directly from a functional liver model, providing rapid and continuous insights into cellular responses and liver function. This capability is particularly critical for studying dynamic processes such as drug-induced liver injury, where timely and continuous data are essential for accurate characterization and intervention. The 3D liver on-a-chip consisted of liver cells encapsulated in a collagen-based extracellular matrix (ECM) and cultured in a dynamic environment mimicking the perfusion flow within physiological liver tissues. The PC-TIR biosensor device, consisting of a multichannel microfluidic chip bonded on the biosensor surface, was connected to a 3D liver on-a-chip model. This technology provided rapid, continuous, label-free, sensitive, and selective monitoring of liver-secreted biomarkers reflecting liver cells' function (albumin) and injury (GST-α). Lastly, we used the fully integrated system to monitor the dynamic response of doxorubicin (DOX)-induced liver toxicity and capture transient drug effects rapidly and continuously.

2. Results and Discussion

2.1 Establishment of the 3D liver on-a-chip model

Compared to other organs, the liver has a unique circulatory system characterized by a dual blood supply from the portal vein and the hepatic artery draining into the central vein and eventually into the hepatic vein [23]. Inspired by the microarchitecture of this vascular system, the design of our 3D liver on-a-chip model recapitulated the circulatory structure of the periportal zone of the liver lobule [24]. The central cell culture chamber, inoculated with HepG2-laden collagen hydrogel, was separated from the microfluidic channels by partial walls with a 300 μm gap that allowed the diffusion of the culture medium in the cell culture chamber (Figure 2a). In our 3D liver on-a-chip model, we used collagen hydrogel to mimic the ECM of the liver, as collagen is one of its major components [25]. The fibrous nature of collagen and its ability to form a gel-like structure significantly contribute to creating a biomimetic microenvironment for HepG2 cells that closely resemble native liver tissues [26]. In the tissue engineering field, collagen hydrogels are widely used to generate 3D models of the liver because they offer a supportive scaffold that facilitates cell attachment, growth, and function [27, 28]. The percentage of collagen used can vary depending on the desired tissue characteristics and the model's complexity. Typically, concentrations of collagen ranging from 1.5 mg/mL to 3 mg/mL are employed to replicate the liver's ECM and provide optimal conditions for hepatocyte function and liver tissue formation [29, 30]. The higher concentrations are often used to create stiffer scaffolds that better mimic the dense ECM of liver tissue, whereas lower concentrations are preferred for studies focusing on cell migration [29]. In our study, we employed a 3 mg/mL concentration of type I collagen to create the scaffold for our liver tissue models. The porosity of collagen gels affects the diffusion behavior of small molecules within the hydrogel matrix [31]. The interconnected porous structure allows for the efficient transport of small molecules, facilitating their movement and interaction within the tissue-engineered environment. This characteristic is essential for simulating physiological conditions, enabling the study of drug diffusion and metabolic processes in liver-on-chip models and other tissue engineering applications [32].

Before inoculating HepG2 cells into the cell culture chamber, we confirmed the diffusion of small molecules throughout the collagen-loaded cell culture chamber while the microfluidic chip was perfused with cell culture media containing 10 kDA FITC-dextran. Within the first hour of perfusion, FITC-dextran was detectable throughout the collagen hydrogel, and the relative fluorescence intensity of FITC steadily increased from 18.9% to 29.2% during the first 8 hours of perfusion and reached saturation thereafter (Figure 2b–c). Although the concentration of FITC-dextran diffusing through the hydrogel was not optimized to represent the liver tissue microenvironment comprehensively, these results confirmed that our 3D liver on-a-chip model loaded with a collagen hydrogel would allow the diffusion and homogeneous distribution of nutrients and drugs from the culture media to support the dynamic culture and treatment of HepG2 cells.

After inoculating HepG2 cells into the cell culture chamber, we assessed their viability, proliferation, and function (albumin secretion) in our 3D liver-on-a-chip model cultured under dynamic conditions for 5 days. The HepG2 cells remained viable, with a 91.5 ± 1.3% viability on day 1 and 96.8 ± 1.2% on day 5 (Figures 2d and 2e). In addition, Cytochrome P450 (CYP) immunostaining was performed to assess the presence and activity of this enzyme before DOX introduction (Figure 2f). The proliferation of HepG2 cells was confirmed by the increased fluorescence of the F-actin staining from day 1 to day 5 of culture, where the growth of cell clusters is evident (Figure 2g). Furthermore, the function of HepG2 cells was maintained throughout the culture period under perfusion. Indeed, HepG2 cells continuously secreted increasing amounts of albumin, from 9.7 ± 1.3 μg/day after 1 day to 115.6 ± 20.3 μg/day after 5 days (Figure 2h). We also demonstrated that HepG2 cells cultured in a dynamic environment secreted significantly higher levels of albumin than HepG2 cells cultured in static conditions on-chip ($p<0.005$) or in a 96-well culture plate ($p<0.0001$) (Figure 2h), confirming that dynamic perfusion culture conditions enhance the secretion of albumin by HepG2 cells, which is one of the most important functions of hepatocytes [27, 33] and a marker of hepatocyte function *in vitro* [27, 33, 34]. These results established that our 3D liver-on-a-chip model remained viable, proliferative, and functional after 5 days of dynamic culture recapitulating the circulatory structure of the periportal zone of the liver lobule. Therefore, we confirmed that our 3D liver-on-a-chip model demonstrated an acceptable baseline functional status to evaluate drug-induced liver toxicity by detecting HepG2-secreted biomarkers in the perfused cell culture medium.

2.2 Fabrication and validation of the microfluidics-integrated PC-TIR biosensor

Assessing the integrity and functionality of OoC models is a costly, time-consuming, labor-intensive process requiring endpoint, invasive, and destructive procedures, which may disrupt the physiological environment and compromise the integrity of the cultured cells [35]. The destructive nature of these methods often provides limited spatial and temporal resolution, which challenges the accuracy of data obtained and compromises the ability to observe real-time and long-term responses and subtle changes at the cellular or molecular level within OoC models [36]. Advancing non-invasive, label-free, and high-resolution monitoring techniques is imperative to provide more accurate and comprehensive data for research, drug development, and personalized medicine applications using OoC models. Therefore, we integrated the PC-TIR biosensor with a microfluidic-based system to enable

streamlined sample routing from the 3D liver on-a-chip model to the biosensor for in-line, label-free, multiplexed, rapid and continuous monitoring of liver cell-secreted biomarkers (Figure 3a).

Although the bonding of polydimethylsiloxane (PDMS) onto the PC-TIR biosensor surface, using O_2 plasma to create hydroxyl groups and facilitate the formation of Si-O-Si covalent bonds, is easy and straightforward, this method does not stop the physical adsorption properties of the PDMS, where small protein molecules would be adsorbed, resulting in reduced biosensing performance [37]. PDMS is known to adsorb proteins [38], trapping small amounts of protein biomarkers before they interact with the biosensor's detection elements. This adsorption effect can increase the response time for detecting a specific biomarker with low concentrations and lower the biosensor's accuracy by detecting lower protein concentrations than actual concentrations in circulation. These inherent properties of PDMS can affect the reliability and precision of biosensors [39].

To address these limitations, we used a silanization modification approach to treat the surfaces of the PDMS and the PC-TIR biosensor to enable the formation of an amine-epoxy bond between them (Figure 3a). The PDMS was treated with (3-aminopropyl)triethoxysilane (APTES) to create the amine functional groups on the surface, while the PC-TIR biosensor was treated with (3-glycidyloxypropyl)trimethoxysilane (GLYMO) to create the epoxy functional groups on the surface [40]. Surface modifications were confirmed using FTIR spectrophotometry on the treated surfaces to observe the presence of the surface functional groups. For the APTES-treated PDMS, the I.R. characteristics 1560–1640 cm^{-1} and 3100–3500 cm^{-1} were observed, corresponding to the bending and stretching of the amine N-H (Figure 3b). The I.R. characteristics of the GLYMO-modified PC-TIR biosensor were observed at 1000–1100 cm^{-1} and 3620–3700 cm^{-1}, corresponding to the epoxy C-O and O-H stretching (Figure 3b). These observations confirmed that the amine and epoxy functional groups were grafted adequately onto the PDMS and PC-TIR biosensor surfaces, respectively. These surface modifications allowed the formation of a covalent bond between the PDMS chip and PC-TIR biosensor, creating a solid seal that prevented leaks and the possibility of cross-contamination between the microchannels on the biosensor, allowing the multiplex detection of biomarkers with one PC-TIR biosensor. Lastly, these surface modifications offered advantages in subsequent antibody functionalization and blocking steps by allowing (1) the direct covalent conjugation between the amine groups on the antibodies and the epoxy functional groups on the PC-TIR biosensor surface and (2) the blocking of the remaining epoxy functional groups by the amine groups found on Bovine serum albumin (BSA). Therefore, the chemistry scheme used to generate the microfluidics-integrated PC-TIR biosensor will not have a negative impact on biomarker detection performances.

To achieve the multiplex detection of biomarkers using the PC-TIR biosensor, we designed a microfluidic channel splitter chip routing the cell culture media from the liver chip to different biosensing microchannels on the PC-TIR biosensor, thus allowing the detection of different liver-secreted biomarkers, namely albumin or GST-α (Figure 3c). We chose albumin as one of the biomarkers for several reasons. Albumin is a major protein synthesized and secreted by the liver, serving as a key indicator of liver function and health.

Its continuous secretion is essential for maintaining osmotic pressure and transporting various substances in the blood. The level of albumin in the culture medium reflects the synthetic capacity of hepatocytes, making it a reliable marker of liver function [41]. In addition, we chose GST-α as a biomarker for liver function and injury over traditional markers such as ALT, AST, and alkaline phosphatase based on several critical factors. GST-α is considered a highly sensitive marker of liver injury, capable of detecting hepatocellular damage even when traditional markers like ALT and AST are within normal ranges. This sensitivity allows for the early identification of liver injury, which is crucial for timely intervention [42]. Additionally, GST-α has been detected in both acute and chronic liver damage, showing a positive correlation with the severity of liver injury [43]. There is also a strong correlation between GST-α levels and liver histopathological endpoints, with GST-α levels rapidly decreasing to baseline after cessation of the drug causing liver injury [44]. These properties make GST-α particularly valuable for monitoring drug-induced liver injury. Through its built-in Y-shaped and straight microchannels, this channel splitter chip distributed the cell culture media equally to the different microchannels of the biosensor chip. Previous studies highlighted the critical role of fluid routing in simulating physiological conditions within organ-on-a-chip models [36, 45, 46]. In the context of liver physiology, the fluid flow within the microfluidic system mimics the circulatory structure of the liver lobule, which is essential for maintaining tissue function and replicating processes like nutrient delivery and waste removal [47–49].

Furthermore, meticulous fluid volume control and dead volume minimization are critical design parameters in developing OoC models. We achieved the integration of the PC-TIR biosensor with a microfluidic system that enabled the controlled routing of cell culture media from the 3D liver on-a-chip model to the PC-TIR biosensor without leaks, bubbles, and disturbance in fluid flow. Using this microfluidic system, avoiding air bubbles in the microfluidic channels was essential, as they can disrupt the sensor’s readings. To prevent bubbles from forming, the tubing connections to the chip must be tight and leak-free, and the tubing must be filled with cell culture media before connecting them to the microfluidic chips.

This microfluidics-integrated PC-TIR biosensor platform is capable of rapid, continuous, in-line, and multiplexed detection of biomarkers secreted by cells cultured in OoC models, but it is limited to detecting four different biomarkers simultaneously. The scalability of this platform for high-throughput screening is a critical consideration for its application in drug toxicity profiling. Potential modifications include increasing the number of parallel microfluidic channels and integrating automated imaging systems for simultaneous real-time monitoring. Such enhancements would enable high-throughput screening capabilities, making the platform more versatile for large-scale applications. To expand the detection capabilities, adjustments such as reducing the size of the microchannels and enhancing the resolution of the complementary metal oxide semiconductor (CMOS) sensor could be investigated. These modifications have the potential to increase the number of biomarkers that can be detected using a single PC-TIR chip. Additionally, smaller microchannels can lead to more efficient use of sample volumes, minimizing the required amount of cell culture media and reagents, which is particularly beneficial for analyzing scarce or valuable biological samples.

2.3 Functionalization and validation of the PC-TIR biosensor

The PC-TIR biosensing device utilized a diode laser as a probe beam to monitor the sensor's resonant angle shift caused by molecules binding to the biosensor's surface (Figure 4a). By utilizing a photonic crystal structure in a total internal reflection configuration, the PC-TIR biosensor provided an open sensing surface with a unique label-free detection mechanism that allows rapid and continuous monitoring of antibody-antigen binding. Conventionally, a sharp resonant condition can be achieved with a high-Q optical microcavity with a cavity layer sandwiched by two pieces of highly reflecting PC structures. However, such a conventional microcavity with a *closed* configuration is not suitable for biosensing because it is difficult for analyte molecules to reach the sensing layer (cavity layer). In contrast, the PC-TIR sensor utilizes only one piece of the PC structure to form an optical microcavity between the high-reflectivity PC structure and the TIR interface [50]. This unique configuration allows a PC-TIR sensor to have a unique *open* microcavity as the sensing surface, which permits the immobilization of monoclonal antibodies (mAbs) on the surface and direct exposure of the functionalized sensor surface to analyte molecules for real-time bioassays [51–53]. Also, most commercially available SPR sensors have a typical bandwidth of ~40 nm [54, 55], whereas a much sharper resonant spectral width (~1–2 nm) can be achieved with a PC-TIR biosensor [50].

PC-TIR sensors can be utilized for a broad range of applications. We demonstrated the applicability of a PC-TIR biosensor for the detection of cardiac troponin I (cTnI) by functionalizing the sensor with anti-cTnI antibody [56] or cTnI-specific aptamers. Our recent study also showed that a PC-TIR sensor can be utilized to monitor conformational changes of a thermo-responsive polymer grafted on the sensor surface [57]. In addition, Nah et al. recently reported the usage of a PC-TIR sensor for rapid and sensitive detection of fentanyl to address the issues of drug misuse and overdose [58]. In our study reported here, we generated PC-TIR biosensors for the detection of albumin and GST-α secreted from a liver-on-a-chip model by utilizing a mAb functionalization process (Figure 4b), where the mAbs were covalently bonded onto a PC-TIR sensor [59]. Since the PC-TIR biosensor surface was pretreated to introduce epoxy functional groups for bonding to the microfluidic chip, the amine groups of the mAbs injected into the microchannel covalently conjugated to the epoxy functional groups of the biosensor surface. Similarly, the amine groups of the BSA used during the blocking step saturated the remaining epoxy functional groups on both the biosensor and PDMS surfaces, thus minimizing the non-specific adsorption of target molecules during biosensing. The blocking step, saturating epoxy functional groups and non-specific binding sites, is crucial for enhancing the detection specificity of biosensors, where the detected signals are solely due to the specific binding of the biomarkers onto the immobilized mAbs [56]. The mAb functionalization and BSA block steps were confirmed by the observation of a significant increase in the shift in the resonant angle of the sensor after deposition of the mAb and BSA layers onto the PC-TIR biosensor surface (data not shown).

We assessed the performance of the PC-TIR biosensors to detect albumin and GST-α simultaneously and in a rapid and continuous manner. The binding of albumin or GST-α to their corresponding antibodies was monitored using the shift in the resonant line

(corresponding to the resonant angle) of the open cavity of the PC-TIR biosensor. The shift was recorded in the unit of pixel number from the image of the reflected probe beam on the CMOS camera. For the rapid and continuous detection of albumin (from 1 to 1,000 ng/mL), we observed an average response time of 277.2 ± 28.2 seconds for all concentrations (Figure 4b), and for the rapid and continuous detection of GST-α (from 1 to 1,000 ng/mL), we observed an average response time of 209.4 ± 70.2 seconds (Figure 4d). Previously reported EC biosensors used for monitoring OoC models typically employed dynamic sampling over hours, where the low temporal resolution could lead to the averaging of instantaneous effects [60]. For example, in a previous study involving the integration of an OoC with an EC biosensor module to detect albumin and GST-α, the measurement could only be made at a sampling rate of >3 hours despite efficient biosensing regeneration capabilities [45]. In contrast, our biosensor can detect and monitor the secretion of several biomarkers at a sampling rate of 3 seconds.

After 20 minutes of continuous detection, the curves of the resonant angle shift did not significantly increase, and sufficient data was acquired to generate an exponential one-phase association model fit to extrapolate the equilibrium signal position, or *Plateau*, that was normalized and used to generate standard curves (Figure S2). We confirmed the reliability of the fitting process, as the average R^2 value of all fittings was >0.95 (Figure S2). The calibration curves indicated a significant correlation between the resonance shift and the concentrations of albumin (R^2= 0.99) and GST-α (R^2= 0.96) in cell culture media (Figure 4 d–f). The calculated detection range for albumin was from 21.68 ng/mL- the limit of detection (LOD)- to 7834.30 ng/mL. For GST-α, the calculated detection range was from 2.198 ng/mL (LOD) to 794.33 ng/mL. The difference in biosensorś performances between the detection of albumin and GST-α is related to the affinity and avidity of the mAbs to their specific antigens. Usually, biosensors using mAbs with high affinity and avidity to their cognate antigen have lower LODs than biosensors using mAbs with low affinity and avidity to their cognate antigen.

Although different running buffers can affect the detection performance of optical biosensors [61–63], our PC-TIR biosensor was optimized and validated using cell culture media as the running buffer. The avidity and affinity of the mAbs used in this study ensure that the antigen-antibody interactions on the biosensor surface generate a signal intensity markedly greater than any noise the running buffer introduces. The selective and high-affinity binding capabilities of the mAbs enhance the detection reliability of our biosensor, even in complex solutions such as cell culture media. Overall, we confirmed that the microfluidics-integrated PC-TIR biosensor could simultaneously detect albumin and GST-α, two liver-secreted biomarkers of function and injury with a response time <5 minutes. These performances are essential for real-time/ near real-time monitoring of drug-induced toxicity in OoC models.

2.4 Rapid and continuous detection of drug-induced liver toxicity using the 3D liver on-a-chip model integrated with a PC-TIR biosensor

The integrated microfluidic system consisted of an in-line sequential connection between a cell culture media reservoir, the 3D liver-on-a-chip model, the splitter chip, the PC-TIR biosensor, and a syringe pump (Figure 1). The syringe pump ensured a steady perfusion

culture by drawing cell culture media from the reservoir through the 3D liver-on-a-chip model, the splitter chip, and the PC-TIR biosensor. This plug-in microfluidic system was user-friendly and required only quick plug-in steps to assemble the entire setup, thus minimizing operator handling. Traditionally, the assembly of integrated OoC platforms is a labor-intensive process with many steps requiring precise manipulations and intricate connections between microfluidic chips [45]. This process could be prone to operator-related variations that can lead to variations in results and outcomes, whereas we demonstrated the seamless integration of an OoC model with a PC-TIR biosensor, providing rapid and continuous monitoring capabilities.

As a proof-of-concept for monitoring liver toxicity, we used DOX, a well-known chemotherapy drug for liver cancer [64], to validate the rapid and continuous detection of drug-induced hepatotoxicity responses using our 3D liver on-a-chip model that used HepG2 cells, a well-established human liver cancer cell line [65]. As a baseline measurement of DOX-induced toxicity, the viability of the 3D liver on-a-chip after 24 hours of DOX exposure was 84.8 ± 4.0% and 76.4 ± 4.6% at concentrations of 5 μM and 20 μM, respectively, whereas without DOX, the viability of the 3D liver on-a-chip was 97.6 ± 0.54% (Figure 5a and b). The viability of HepG2 cells was significantly lower when treated with 5 μM ($p<0.001$) and 20 μM ($p<0.001$) compared to untreated cells. Moreover, the level of albumin secreted by the 3D liver on-a-chip after 24 hours of DOX treatment did not significantly change ($p=0.10$) (Figure 5c), consistent with previous findings in the literature [66, 67]. In contrast, the secretion of GST-α significantly increased when the 3D liver on-a-chip was treated with 20 μM DOX than without DOX (4.54 ng/mL vs. 1.59 ng/mL, $p<0.001$) (Figure 5d). Although the levels of GST-α were not significantly higher ($p=0.29$) when the 3D liver on-a-chip was treated with 5 μM DOX compared to that without DOX treatments, a slight increase was observed from 0.76 ± 0.24 to 1.59 ± 0.63 ng/mL. GST-α is an enzyme secreted by hepatocytes during hepatotoxicity, and elevated levels of GST-α are associated with liver injury [68]. Also, GST-α has been suggested as a viable biomarker of impaired liver function and drug-induced liver hepatotoxicity [69, 70]. Therefore, monitoring the secretion of GST-α is an appropriate approach to detecting drug-induced liver toxicity in the 3D liver on-a-chip. More specifically, we confirmed that, with respect to DOX treatment for 24 hours, there was a significant correlation between the viability of HepG2 cells and the levels of GST-α detected by ELISA ($p=0.04$), whereas no significant correlation was observed between the viability of HepG2 cells and the levels of albumin ($p=0.19$) (Table S1). As a result, we confirmed that, in our 3D liver on-a-chip model, the secreted GST-α levels could indicate HepG2 cell healthy state and viability.

We used our microfluidics-integrated PC-TIR biosensor to rapidly and continuously monitor the DOX-induced hepatotoxicity responses in our 3D liver on-a-chip model. The PC-TIR biosensor detected HepG2-secreted albumin after 40.05 ± 0.16 minutes. After 6 hours of DOX treatment, significant differences in albumin levels between DOX-treated and untreated 3D liver on-a-chip were observed (Figure 5d). Specifically, a significant increase in albumin secretion was observed when the 3D liver on-a-chip was treated with 20 μM DOX compared to the control group (0 μM DOX) ($p<0.002$). This significant increase in albumin was observed after 60 minutes of DOX treatment and remained significant for 6 hours (Table S2). In contrast, albumin levels were not significantly different between

the group treated with 5-μM DOX and the control group ($p<0.85$). Moreover, the PC-TIR biosensor detected HepG2-secreted GST-α after 90.68 ± 0.72 minutes. We observed a significant increase in HepG2-secreted GST-α when treated with 20 μM of DOX for 6 hours compared to untreated ($p<0.001$) or 5 μM DOX-treated ($p<0.005$) 3D liver on-a-chip (Figure 5d). This significant increase in GST-α was observed after 160 minutes of DOX treatment and remained significant for 6 hours (Table S3). However, the secretion of GST-α was not significantly different between the group treated with 5 μM DOX and the control group ($p<0.39$).

Interestingly, albumin secretion was detected after 40 minutes, whereas GST-α secretion was detected 2 hours after 20 μM DOX treatment (Figure 5d). Since albumin is continuously secreted by HepG2 cells, we anticipated that albumin would be detected rapidly and before GST-α. However, we observed a 40-minute delay in detection that could be caused by several factors, including cell acclimatization, perfusion velocity, and diffusion through the collagen matrix. The latter could act as a physical barrier that significantly delays the detection of cell-secreted biomarkers, as well as the diffusion dynamics of DOX in the cell culture chamber, which could also influence the 2-hour response observed with GST-α. Indeed, collagen hydrogels slow down the penetration of DOX into the liver tissue constructs (as observed in our FITC-dextran diffusion experiments in Figure 2b–c), leading to a potentially delayed cellular uptake and response (i.e., GST-α secretion). These observations highlight the importance of considering the physical constraints imposed by the 3D liver on-a-chip model, and such diffusion-related challenges must be acknowledged for an accurate assessment of drug-response dynamics.

In addition, despite the promising results, our study has several limitations. One major challenge is the diffusion rates of molecules within the collagen matrix, which can delay the detection of cell-secreted biomarkers. This delay can affect the rapid monitoring capability of our system. Also, the *distance between* the culture and monitoring units poses another challenge. The physical distance between the culture chamber and the biosensor can lead to deviations in the detected biomarker concentrations compared to their actual levels in the culture chamber. Future improvements will aim to reduce these physical separations and optimize the diffusion dynamics within the system to enhance the accuracy and responsiveness of the platform. However, compared to the viability measurements after 24 hours of DOX treatment using fluorescent imaging and traditional endpoint assays, our integrated microfluidic system demonstrated the ability for fast, and continuous *in situ* monitoring of liver-secreted biomarkers in response to drug treatment.

Overall, our 3D liver on-a-chip model integrated with a PC-TIR biosensor exhibits many advantages for biomedical research, including mechanistic insights into disease biology, reduced experimental variability, and temporal dynamics analysis for disease modeling, drug discovery, and personalized medicine applications.

3. CONCLUSIONS

We developed a plug-in solution concept that integrates a PC-TIR optical biosensor with a liver-on-a-chip model for label-free, rapid and continuous monitoring of secreted biomarkers

due to drug toxicity. This PC-TIR biosensing system achieved continuous and *in situ* monitoring, thereby enabling the rapid detection of DOX-induced liver toxicity responses. In summary, we provide a novel approach for in-line sensing applications in organ-on-a-chip using an advanced optical PC-TIR biosensor for label-free, rapid and continuous monitoring. It has been demonstrated that this sensing platform could be compatible with other existing organ-on-a-chip models and dynamically track their biochemical parameters for drug screening by providing rapid, continuous, *in situ* microenvironment monitoring.

4. Experimental Section/Methods

Design and fabrication of the microfluidic devices:

Design of the liver chip device: The liver chip design was inspired by the microarchitecture of the liver sinusoid, where two input microchannels (hepatic artery and portal vein) converge to a single output (central vein) having a liver cell culture microchamber between the input channels. The microchannels were 800 μm high and 1 mm wide, and the microchamber was 800 μm high and 500 μm wide. The microchannels and microchamber were separated by partial walls (500 μm high and 750 μm wide), allowing the transfer of gel solutions or cell culture media in the different compartments of the microfluidic device.

Design of the microchannel splitter chip and the biosensing chip: The biosensing chip comprised 5 microchannels, of which one microchannel was used as the control channel for internal calibration of the PC-TIR biosensor, two microchannels were used for the detection of one biomarker (i.e., albumin), and the last two microchannels for the detection of another biomarker (i.e., GST-α). The microchannels of the biosensing chip were 200 μm high, 1.8 mm wide, and 10 mm long, with a spacing of 1.4 mm between them. The microchannel splitter chip consisted of one straight microchannel and two Y-shaped microchannels. The straight microchannel was used to route the control solution to the control microchannel of the biosensing chip. The Y-shaped microchannels were used to route the cell culture media from the liver chip to the biosensing microchannels to detect the first and second biomarkers, namely albumin and GST-α. The microchannels of the splitter chip were 200 μm high, 1.8 mm wide, and 10 mm long, with a spacing of 2 mm between them. *(3) Fabrication of the PDMS-based microfluidic chips:*

The 3D model of a master negative mold for each microfluidic device was generated using a computer-aided design modeling software (SolidWorks 2021). The 3D models were exported to a liquid crystal display (LCD) 3D printer (Halot-Mage Pro, Creality), and the master molds were printed with fast ultraviolet curable resin (Creality) with a printing resolution of 8K (7680 × 4320). Once printed, both surfaces of the molds were exposed to UV light with a power of 9.9 J (13-245-221, Fisher Scientific) for 1 hour, then thermally treated at 60°C overnight to prevent the adhesion of PDMS to the resin and allow the reuse of the master mold. After curing the molds, a 10:1 ratio mixture of PDMS base and curing agent (Sylgard 184, Dow Corning) was poured into the molds. The PDMS-filled molds were degassed in a desiccator to remove air bubbles and cured in an oven at 60°C overnight. The cured PDMS chips were carefully removed from the molds, and 1.5 mm

holes were punched at the end of each microchannel for all microfluidic devices. Next, the PDMS chips were cleaned with ethanol and deionized water in an ultrasonic bath for 10 minutes and then dried with nitrogen gas. The liver chip and the microchannel splitter chip were bonded to clean 75 mm × 25 mm and 25 mm × 25 mm glass slides, respectively, using a 3-minute O_2 plasma treatment (PE-25, Plasma Etch). The microchannel device was covalently bonded to the PC-TIR biosensor using an amine-epoxy reaction. Briefly, the PC-TIR biosensor surface was activated with O_2 plasma for 5 minutes and then immersed in a 2% (3-glycidyloxypropyl)trimethoxysilane (GLYMO) solution in toluene at 60°C for 6 hours for epoxy functional group modification. The surface of the microchannel device was activated with O_2 plasma for 5 minutes and then immersed in a 2% APTES solution in ethanol for 1 hour at 60°C for amine functional group modification. After surface modification, the PC-TIR biosensor and the PDMS microchannel device were thoroughly rinsed with ethanol and water and then dried with nitrogen gas. Finally, they were attached and cured in an oven at 60°C for 3 hours. The surface modifications were characterized and confirmed using an FTIR spectrometer (ALPHA II, Bruker), with spectral analysis ranging from 5000 cm^{-1} to 400 cm^{-1} with a resolution of 4 cm^{-1}. Lastly, the device was sterilized with 70% ethanol, rinsed with 1X DPBS, and exposed to UV light for 1 hour before usage or storage in a humidity-controlled environment until use.

Establishment of the 3D liver-on-a-chip model: HepG2 liver cells (HB-8065, ATCC) were cultured in Dulbecco's modified Eagle's medium (DMEM, 10569–010, Gibco) supplemented with 10% fetal bovine serum (FBS) (Gibco) and 1% penicillin-streptomycin (15140–122, Gibco). The cells were cultured at 37°C and 5% CO_2 in a humidified incubator, with media replacement every 2–3 days. In all the experiments, HepG2 cells between passages 16–25 were used. Upon reaching 80% confluence, the cells were detached using 0.05% trypsin-EDTA (25200–056, Gibco). Then, HepG2 cells were resuspended in a 3 mg/mL type I collagen (ALX-522-435-0100, Enzo) solution at a concentration of 1×10^6 cells/mL. The cell-loaded collagen solution (60 μL) was gently injected into the microchamber of a sterile liver chip device and allowed to polymerize at 37°C for 30 minutes. The injection port was then sealed with parafilm to prevent evaporation, and culture media was added to the microchannels. The liver chip was connected with sterile Tygon tubing (06419, Masterflex™) to a syringe pump and a sterile media reservoir, perfused at a flow rate of 1.5 μL/min, and cultured at 37°C with 5% CO_2 for 5 days (Figure S1). Cell viability was assessed using the LIVE/DEAD® Viability/Cytotoxicity Kit (L3224, Invitrogen) and nuclear staining with Hoechst 33342 (H3570, Invitrogen) with working concentrations of 2 μM, 4 μM, and 5 μg/mL, respectively. The 3D liver-on-a-chip was rinsed with 1X DPBS and stained for 45 minutes. After staining, the chips were washed three times with 1X DPBS before imaging. Fluorescent images were captured using a confocal microscope (Axio Observer LSM 710, Carl Zeiss) and analyzed using FIJI (version 1.54f, ImageJ) image analysis software. Cell viability was calculated by measuring the EthD-1 signal (dead cells) relative to the total number of cells identified by Hoechst staining. To visualize the cytoskeleton, the chips were stained for F-actin using rhodamine-phalloidin. Briefly, the chips were fixed overnight at 4°C using a 4% paraformaldehyde solution. Then, the chips were washed 3 times for 30 minutes with 1X DPBS and incubated with a 1:200 dilution of phalloidin-Alexa 647 (A22287, Invitrogen) and Hoechst 33342 overnight at 4°C.

The chips were washed with DPBS and stored in the dark at 4°C before confocal imaging. Lastly, 2.16 mL of cell culture medium was collected from the outlet of the chips daily for 5 days to evaluate the functionality of the 3D liver on-a-chip model. To assess the impact of dynamic culture conditions on the functionality of HepG2 cells, we cultured the 3D liver on-a-chip under static conditions where the chip was cultured in 90 μL of cell culture media with the entire volume being collected and refreshed daily for 5 days. Similarly, we performed static culture experiments in 96-well plates where 60 μL of HepG2 cell-loaded collagen solution was carefully pipetted into each well and cultured with 90 μL of cell culture media that was collected and refreshed daily for 5 days. Albumin secretion levels were quantified using a human albumin ELISA kit (DY1455, R&D Systems) according to the manufacturer's protocol. Absorbance readings at 450 nm, with a 570 nm reference, were obtained using a microplate reader (Varioskan LUX, Thermo Fisher).

Cytochrome P450 (CYP) immunostaining was performed to assess the presence and activity of liver-detoxifying enzymes in the 3D liver-on-a-chip model. HepG2 cell-loaded collagen was fixed with 4% paraformaldehyde for 15 minutes, followed by permeabilization with 0.1% Triton X-100 (HFH10, Thermo Fisher) for 10 minutes. After blocking with 1% BSA for 1 hour at room temperature, the cells were incubated overnight at 4°C with primary antibodies against CYP (JM44–23, Thermo Fisher) diluted in blocking solution (1% BSA). The following day, the cells were washed three times with PBS and incubated with Alexa Fluor-conjugated secondary antibodies (ab150075, Abcam) for 1 hour at room temperature. Nuclei were counterstained with Hoechst. Fluorescence images were captured using a confocal microscope to confirm the expression of the CYP enzyme.

Evaluation of small molecule diffusion through the collagen matrix of the 3D liver on-a-chip model: To evaluate the diffusion of small molecules through the collagen-based 3D liver on-a-chip model, 10-kDa FITC-dextran solution (FD10S, Sigma-Aldrich) was perfused through the chip. The microchamber of the 3D liver on-a-chip was loaded with 60 μL of type I collagen solution (3 mg/mL) and incubated at 37°C for 30 minutes to allow the polymerization of the collagen-based hydrogel matrix. Before starting the diffusion experiments, the channels of the chip were prefilled with 1X DPBS and equilibrated for 1 hour at room temperature to saturate the collagen hydrogel matrix. Next, a 0.5 mg/mL FITC-dextran solution was perfused through the chip at a controlled flow rate of 1.5 μL/min using a syringe pump (NE-1200, New Era Pump Systems). The diffusion process was observed with time-lapse fluorescence imaging using a fluorescence microscope (ECHO Revolve, ECHO). The acquired fluorescence intensity data were quantified using FIJI (version 1.54f, ImageJ) image analysis software.

PC-TIR Biosensor chip and its optical monitoring system: The fabrication of PC-TIR biosensors has been described in detail in previous studies [56, 71, 72]. Briefly, the PC-TIR biosensor chip consists of a thin-film structure with 5 layers of dielectric coatings with alternating layers between 90.6-nm titanium dioxide (TiO2) and 308.8-nm silicon dioxide (SiO_2), deposited using electron beam physical vapor deposition on a BK7 glass substrate. A 3-nm silicon layer and a 377.1-nm SiO_2 layer were further coated on top of the alternating layers to create a unique optical microcavity for a probe beam at 650 nm

with an incident angle of 64 degrees (above the critical angle for TIR). The formed optical microcavity has a unique open structure due to TIR (without substrate or materials coated on top of the cavity layer), thus allowing the PC-TIR sensor chip to easily integrate with microfluidic-based chips and detect specific analytes [73, 74]. An optical imaging system was developed to monitor the changes in the PC-TIR sensor's resonant angle due to binding events on the sensor surface. The system utilized a compact diode laser with an output wavelength of 650 nm as a probe beam for the biosensor. The beam was first expanded to 20 mm wide and then focused with a cylindrical lens into a line on the sensor chip coupled with a BK7 equilateral prism. A CMOS camera was then used to capture the reflected light from the sensor chip. A resonant angle was observed, and its peak location was precisely determined using a Lorentzian function to fit the intensity profile of the reflected probe beam recorded by the CMOS camera. Quantification of antibody-antigen interactions can be obtained by analyzing the pixel shift of the resonant line on the recorded images. Before placing the biosensing chip onto the prism, the surface of the biosensing chip was cleaned with a lens cleaner liquid (no. 1 for coated optics, Lens Clen). A drop of index-matching liquid (IML 150, Norland) was then applied to the prism to couple the biosensor chip. The biosensor chip was also integrated with a microfluidic system linked with Tygon tubing to flow the cell culture media from the 3D liver on-a-chip to the biosensor chip via the microchannel splitter chip using a syringe pump.

Functionalization of the PC-TIR Biosensor: First, 1X DPBS solution was perfused through the microchannels for 5 minutes at a 20 μL/min flow rate to clean and stabilize the PC-TIR biosensor surface. Monoclonal antibodies (mAbs) were then covalently immobilized onto the surface of the PC-TIR biosensor using click reactions between epoxy-activated surface and amino groups of antibodies. Briefly, 10 μL of 100 μg/mL anti-albumin (MA5–29022, Invitrogen) or anti-GSTA1 (H00002938-M01, Abnova) mAbs were added to the microchannels of the PC-TIR biosensor chip and incubated overnight at 4°C. The microchannels were washed three times with 1X DPBS to remove unbound antibodies, and then they were blocked with a 1% BSA solution for 1 hour to prevent non-specific protein adsorption. After the blocking step, the microchannels were washed with 1X DPBS and used immediately or stored at 4°C for use the next day. The changes in the response signal of the PC-TIR biosensor before and after functionalization and blocking were measured with a sampling rate of 3 seconds. The immobilization of mAbs on the sensor surface was confirmed by the resonant angle shift via recording the corresponding resonant line shift (in the unit of pixel numbers) on the images, while a control microchannel was used to establish the baseline resonant shift and normalize the results from other microchannels.

Validation of the dynamic, rapid, and continuous detection of albumin and GST-α: The detection of albumin and GST-α using the PC-TIR biosensor was performed under dynamic flow conditions. First, the microchannels of the biosensor were perfused with cell culture media at a flow rate of 5 μL/min to stabilize the PC-TIR biosensor surface and the resonant shift signal for each channel. One of the microchannels was assigned as the control channel, with a continuous flow of cell culture media applied throughout the experiment for calibration and to compensate for any baseline offset. The other channels were perfused with cell culture media spiked with different concentrations (1, 10, 100, and

1000 ng/mL) of human albumin (A9611, Sigma-Aldrich) and GST-α recombinant proteins (HY-P75153A, MedChem Express) for 20 minutes. Although the culture medium used in our experiments contained bovine serum albumin, in albumin detection, the antibody used for functionalizing the sensor had specificity to human serum albumin. Nevertheless, the resonant shift of the control channel, which contains the same medium used in the experimental channel, was subtracted from the resonant shift of each experimental channel, effectively normalizing the data. This normalization step ensured that the detected signals accurately reflected the albumin secreted by the HepG2 cells.

We applied an exponential one-phase association model to fit the normalized and time-dependent resonant shift data. The fitting process was run automatically using GraphPad Prism to determine the variation in antibody-antigen binding at different concentrations. The equation used for fitting is as follows: $IF(X < X_0, Y_0, Y_0 + (Plateau - Y_0) \times (1 - exp(-K \times (X - X_0))))$. Here, X_0 is the initial time of binding, Y_0 is the baseline signal position, *Plateau* is the equilibrium signal position, and K is the rate constant to reach this equilibrium. The difference between *Plateau* and Y_0 was used to represent the analyte's concentration. Since optical biosensors generate signals that fit the sigmoidal curve [75], we generated standard curves for the detection of albumin and GST-α using dose-response curves models generated in GraphPad Prism using the following equation: $Y = Bottom + (Top - Bottom)/(1 + 10\text{^}(LogEC50 - X))$. Here, *Top* and *Bottom* are plateaus in the units of the Y axis (response shift in pixels), EC50 is the concentration of analyte that gives a response halfway between *Bottom* and *Top*, and X is the logarithm of DOX concentrations. To determine the detection range of the PC-TIR biosensor, we calculated the lower limit DOX concentration corresponding to a response shift in pixels that is 5% of the Span (=*Top*-*Bottom*) above the *Bottom* value and the upper limit DOX concentration corresponding to a response shift in pixels that is 95% of the Span above the *Bottom* value.

Drug Treatment and rapid and continuous detection of liver toxicity: To evaluate drug toxicity, the 3D liver on-a-chip model was treated with DOX (Sigma-Aldrich), and the in-line PC-TIR biosensor was used for *in situ* and rapid and continuous measurements of liver-secreted biomarkers, namely albumin (as a measure of liver function) and GST-α (as a measure of liver injury). Briefly, the 3D liver on-a-chip was perfused for 2 days to establish a stable microenvironment before drug exposure. DOX was then perfused at concentrations of 0 (control), 5, and 20 μM for 24 hours. During this time, the PC-TIR biosensor was utilized to continuously monitor the levels of albumin and GST-α secreted by the liver cells in response to DOX. Following the DOX treatment, cell viability was assessed using the LIVE/DEAD® Viability/Cytotoxicity Kit, while albumin and GST-α secretion levels were measured using ELISA kits. The results were compared with the data obtained with the PC-TIR biosensor.

Statistical analysis: All statistical analyses were performed using the GraphPad Prism 9 software. Results are expressed as mean ± standard deviation from triplicate experiments. All data was tested for normality using the Shapiro-Wilk and Shapiro-Francia tests. When applicable, analyses for significance were performed using a parametric or non-parametric

analysis of variance (ANOVA) test, followed by Tukey's test for multiple comparisons. We used a pairwise correlation analysis to examine the correlation between HepG2 viability, albumin levels, and GST-α levels when treated with DOX. The area under the curve was calculated using the area under the curve analysis (AUC) in Prism 9 software, where response shift (pixel) was plotted in function of time, and the resulting function was used to calculate the AUC. Statistical significance was defined by $p<0.05$ for two-sided p-values. Significance levels were as follows: * for $p < 0.05$, ** for $p < 0.01$, and *** for $p < 0.001$.

Supplementary Material

Refer to Web version on PubMed Central for supplementary material.

ACKNOWLEDGMENTS

The authors acknowledge funding from the National Institutes of Health (TR003148 and GM126571). J.-W. Y. acknowledges financial support from the National Science and Technology Council (NSTC 112-2917-I-564-015), Taiwan.

REFERENCES

1. Leung CM; de Haan P; Ronaldson-Bouchard K; Kim G-A; Ko J; Rho HS; Chen Z; Habibovic P; Jeon NL; Takayama S; Shuler ML; Vunjak-Novakovic G; Frey O; Verpoorte E; Toh Y-C, Nature Reviews Methods Primers 2022, 2 (1), 33. DOI 10.1038/s43586-022-00118-6.
2. Ma C; Peng Y; Li H; Chen W, Trends in pharmacological sciences 2021, 42 (2), 119–133. [PubMed: 33341248]
3. Si L; Bai H; Rodas M; Cao W; Oh CY; Jiang A; Moller R; Hoagland D; Oishi K; Horiuchi S; Uhl S; Blanco-Melo D; Albrecht RA; Liu W-C; Jordan T; Nilsson-Payant BE; Golynker I; Frere J; Logue J; Haupt R; McGrath M; Weston S; Zhang T; Plebani R; Soong M; Nurani A; Kim SM; Zhu DY; Benam KH; Goyal G; Gilpin SE; Prantil-Baun R; Gygi SP; Powers RK; Carlson KE; Frieman M; tenOever BR; Ingber DE, Nature Biomedical Engineering 2021, 5 (8), 815–829. DOI 10.1038/s41551-021-00718-9.
4. Bai H; Si L; Jiang A; Belgur C; Zhai Y; Plebani R; Oh CY; Rodas M; Patil A; Nurani A; Gilpin SE; Powers RK; Goyal G; Prantil-Baun R; Ingber DE, Nature Communications 2022, 13 (1), 1928. DOI 10.1038/s41467-022-29562-4.
5. Aleman J; Skardal A, Biotechnology and Bioengineering 2019, 116 (4), 936–944. DOI 10.1002/bit.26871. [PubMed: 30450540]
6. Conceição F; Sousa DM; Loessberg-Zahl J; Vollertsen AR; Neto E; Søe K; Paredes J; Leferink A; Lamghari M, Materials Today Bio 2022, 13, 100219.
7. Herland A; Maoz BM; Das D; Somayaji MR; Prantil-Baun R; Novak R; Cronce M; Huffstater T; Jeanty SSF; Ingram M; Chalkiadaki A; Benson Chou D; Marquez S; Delahanty A; Jalili-Firoozinezhad S; Milton Y; Sontheimer-Phelps A; Swenor B; Levy O; Parker KK; Przekwas A; Ingber DE, Nature Biomedical Engineering 2020, 4 (4), 421–436. DOI 10.1038/s41551-019-0498-9.
8. Petreus T; Cadogan E; Hughes G; Smith A; Pilla Reddy V; Lau A; O'Connor MJ; Critchlow S; Ashford M; Oplustil O'Connor L, Communications Biology 2021, 4 (1), 1001. DOI 10.1038/s42003-021-02526-y. [PubMed: 34429505]
9. Reyes DR; Esch MB; Ewart L; Nasiri R; Herland A; Sung K; Piergiovanni M; Lucchesi C; Shoemaker JT; Vukasinovic J, Lab on a Chip 2024.
10. Mansouri M; Lam J; Sung KE, Lab on a Chip 2024.
11. Ewart L; Apostolou A; Briggs SA; Carman CV; Chaff JT; Heng AR; Jadalannagari S; Janardhanan J; Jang K-J; Joshipura SR; Kadam MM; Kanellias M; Kujala VJ; Kulkarni G; Le CY; Lucchesi C; Manatakis DV; Maniar KK; Quinn ME; Ravan JS; Rizos AC; Sauld JFK; Sliz JD; Tien-Street W; Trinidad DR; Velez J; Wendell M; Irrechukwu O; Mahalingaiah PK; Ingber DE; Scannell

JW; Levner D, Communications Medicine 2022, 2 (1), 154. DOI 10.1038/s43856-022-00209-1. [PubMed: 36473994]

12. Zhu Y; Mandal K; Hernandez AL; Kawakita S; Huang W; Bandaru P; Ahadian S; Kim H-J; Jucaud V; Dokmeci MR; Khademhosseini A, Current Opinion in Biomedical Engineering 2021, 19, 100309. DOI 10.1016/j.cobme.2021.100309. [PubMed: 37206309]
13. Fernandez-Checa JC; Bagnaninchi P; Ye H; Sancho-Bru P; Falcon-Perez JM; Royo F; Garcia-Ruiz C; Konu O; Miranda J; Lunov O, Journal of Hepatology 2021, 75 (4), 935–959. [PubMed: 34171436]
14. Weaver RJ; Blomme EA; Chadwick AE; Copple IM; Gerets HHJ; Goldring CE; Guillouzo A; Hewitt PG; Ingelman-Sundberg M; Jensen KG; Juhila S; Klingmüller U; Labbe G; Liguori MJ; Lovatt CA; Morgan P; Naisbitt DJ; Pieters RHH; Snoeys J; van de Water B; Williams DP; Park BK, Nature Reviews Drug Discovery 2020, 19 (2), 131–148. DOI 10.1038/s41573-019-0048-x. [PubMed: 31748707]
15. Mou L; Mandal K; Mecwan MM; Hernandez AL; Maity S; Sharma S; Herculano RD; Kawakita S; Jucaud V; Dokmeci MR, Lab on a Chip 2022, 22 (20), 3801–3816. [PubMed: 36074812]
16. Das S; Devireddy R; Gartia MR, Biosensors 2023, 13 (3), 396. [PubMed: 36979608]
17. Singh AK; Anwar M; Pradhan R; Ashar MS; Rai N; Dey S, Journal of Biophotonics 2023, 16 (7), e202200380. [PubMed: 36883612]
18. Acharya B; Behera A; Behera S, Chemical Physics Impact 2024, 8, 100414.
19. Sugai H; Tomita S; Ishihara S; Yoshioka K; Kurita R, Analytical Chemistry 2020, 92 (22), 14939–14946. DOI 10.1021/acs.analchem.0c02220. [PubMed: 33112611]
20. Shevchenko Y; Camci-Unal G; Cuttica DF; Dokmeci MR; Albert J; Khademhosseini A, Biosensors and Bioelectronics 2014, 56, 359–367. DOI 10.1016/j.bios.2014.01.018. [PubMed: 24549115]
21. Konoplev G; Agafonova D; Bakhchova L; Mukhin N; Kurachkina M; Schmidt M-P; Verlov N; Sidorov A; Oseev A; Stepanova O, Biomedicines 2022, 10 (2), 207. [PubMed: 35203416]
22. Syahir A; Usui K; Tomizaki K.-y.; Kajikawa K; Mihara H, Microarrays 2015, 4 (2), 228–244. [PubMed: 27600222]
23. Nagy P; Thorgeirsson SS; Grisham JW, The Liver: Biology and Pathobiology 2020, 1–13.
24. Moradi E; Jalili-Firoozinezhad S; Solati-Hashjin M, Acta biomaterialia 2020, 116, 67–83. [PubMed: 32890749]
25. Karsdal MA; Daniels SJ; Holm Nielsen S; Bager C; Rasmussen DG; Loomba R; Surabattula R; Villesen IF; Luo Y; Shevell D, Liver International 2020, 40 (4), 736–750. [PubMed: 31997561]
26. Chen L; Ma H; Li K; Song X; Zeng X, Materials Science and Engineering: C 2021, 126, 112119. [PubMed: 34082936]
27. Polidoro MA; Ferrari E; Marzorati S; Lleo A; Rasponi M, Liver international 2021, 41 (8), 1744–1761. [PubMed: 33966344]
28. Mi S; Yi X; Du Z; Xu Y; Sun W, Biofabrication 2018, 10 (2), 025010. [PubMed: 29460846]
29. Alevra Sarika N; Payen VL; Fléron M; Ravau J; Brusa D; Najimi M; De Pauw E; Eppe G; Mazzucchelli G; Sokal EM, Cells 2020, 9 (6), 1357. [PubMed: 32486126]
30. LeCluyse EL; Alexandre E; Hamilton GA; Viollon-Abadie C; Coon DJ; Jolley S; Richert L, Basic Cell Culture Protocols 2005, 207–229.
31. Antoine EE; Vlachos PP; Rylander MN, PloS one 2015, 10 (3), e0122500. [PubMed: 25822731]
32. Ye S; Boeter JW; Penning LC; Spee B; Schneeberger K, Bioengineering 2019, 6 (3), 59. [PubMed: 31284412]
33. Chen Y; Tang D; Wu H; Wu Y; Yuan T; Zhang H; Jiao Y; Yu W; Yan H, Archives of Toxicology 2021, 95, 2431–2442. [PubMed: 33852043]
34. Török G; Erdei Z; Lilienberg J; Apáti Á; Homolya L, PLoS One 2020, 15 (1), e0227751. [PubMed: 31971960]
35. Fuchs S; Johansson S; Tjell AØ; Werr G; Mayr T; Tenje M, ACS Biomaterials Science & Engineering 2021, 7 (7), 2926–2948. [PubMed: 34133114]
36. Azizgolshani H; Coppeta J; Vedula E; Marr E; Cain B; Luu R; Lech M; Kann S; Mulhern T; Tandon V, Lab on a Chip 2021, 21 (8), 1454–1474. [PubMed: 33881130]

37. Shakeri A; Khan S; Didar TF, Lab on a Chip 2021, 21 (16), 3053–3075. DOI 10.1039/D1LC00288K. [PubMed: 34286800]
38. Van Meer B; de Vries H; Firth K; van Weerd J; Tertoolen L; Karperien H; Jonkheijm P; Denning C; IJzerman A; Mummery C, Biochemical and biophysical research communications 2017, 482 (2), 323–328. [PubMed: 27856254]
39. Yao J; Guan Y; Park Y; Choi YE; Kim HS; Park J, Sensors 2021, 21 (5), 1754. [PubMed: 33806281]
40. Tang L; Lee NY, Lab on a Chip 2010, 10 (10), 1274–1280. DOI 10.1039/B924753J. [PubMed: 20445880]
41. Sun L; Yin H; Liu M; Xu G; Zhou X; Ge P; Yang H; Mao Y, Annals of medicine 2019, 51 (7–8), 333–344. [PubMed: 31714153]
42. Czuczejko J; Mila-Kierzenkowska C; Szewczyk-Golec K, Canadian Journal of Gastroenterology and Hepatology 2019, 2019 (1), 5850787. [PubMed: 31772928]
43. Cueto-Sánchez A; Niu H; Álvarez-Álvarez I; López-Longarela B; Del Campo-Herrera E; Ortega-Alonso A; García-Cortés M; Pinazo-Bandera J; Sanabria-Cabrera J; Díaz-Mochón JJ, British Journal of Clinical Pharmacology 2023, 89 (8), 2497–2507. [PubMed: 36965054]
44. Teo SH; Endre ZH, Best Practice & Research Clinical Anaesthesiology 2017, 31 (3), 331–344. DOI 10.1016/j.bpa.2017.10.003. [PubMed: 29248140]
45. Zhang YS; Aleman J; Shin SR; Kilic T; Kim D; Mousavi Shaegh SA; Massa S; Riahi R; Chae S; Hu N, Proceedings of the National Academy of Sciences 2017, 114 (12), E2293–E2302.
46. Coppeta J; Mescher M; Isenberg B; Spencer A; Kim E; Lever A; Mulhern T; Prantil-Baun R; Comolli J; Borenstein J, Lab on a Chip 2017, 17 (1), 134–144.
47. Du Y; Li N; Yang H; Luo C; Gong Y; Tong C; Gao Y; Lü S; Long M, Lab on a Chip 2017, 17 (5), 782–794. [PubMed: 28112323]
48. Meng Q; Wang Y; Li Y; Shen C, Biotechnology and Bioengineering 2021, 118 (2), 612–621. [PubMed: 33017042]
49. Menezes PD; Gadegaard N; Natal Jorge RM; Pinto SI, International Journal for Numerical Methods in Biomedical Engineering 2021, 37 (5), e3445. [PubMed: 33522149]
50. Guo Y; Divin C; Myc A; Terry FL; Baker JR; Norris TB; Ye JY, Optics express 2008, 16 (16), 11741–11749. [PubMed: 18679444]
51. Zhang B; Morales AW; Peterson R; Tang L; Ye JY, Biosensors & bioelectronics 2014, 58, 107–13. DOI 10.1016/j.bios.2014.02.057. [PubMed: 24632136]
52. Zhang B; Dallo S; Peterson R; Hussain S; Weitao T; Ye JY, J Biomed Opt 2011, 16 (12), 127006. DOI 10.1117/1.3662460. [PubMed: 22191936]
53. Zhang B; Wang B; Morales AW; Scudder J; Bhattacharyya MK; Ye JY, Analytical chemistry 2016, 88 (6), 3024–30. DOI 10.1021/acs.analchem.5b02442. [PubMed: 26859241]
54. Homola J, Chemical Reviews 2008, 108 (2), 462–493. DOI Doi 10.1021/Cr068107d. [PubMed: 18229953]
55. Hoa XD; Kirk AG; Tabrizian M, Biosensors & bioelectronics 2007, 23 (2), 151–160. DOI DOI 10.1016/j.bios.2007.07.001. [PubMed: 17716889]
56. Zhang B; Morales AW; Peterson R; Tang L; Ye JY, Biosensors and Bioelectronics 2014, 58, 107–113. [PubMed: 24632136]
57. Trabucco L; Guess H; Ulloa JC; Ahmed M; McFadden S; Guntnur RT; Akimov N; Romero G; Ye JY In Label-free quantification of POEGMA-144 polymerization and thermal response via PC-TIR biosensor, Label-free Biomedical Imaging and Sensing (LBIS) 2023, SPIE: 2023; pp 99–104.
58. Nah SH; Unsihuay D; Wang P; Yang S, ACS applied materials & interfaces 2023, 15 (23), 27647–27657. [PubMed: 37252783]
59. Gao S; Guisán JM; Rocha-Martin J, Analytica Chimica Acta 2022, 1189, 338907. DOI 10.1016/j.aca.2021.338907. [PubMed: 34815045]
60. Ortega MA; Fernández-Garibay X; Castaño AG; De Chiara F; Hernández-Albors A; Balaguer-Trias J; Ramón-Azcón J, Lab on a Chip 2019, 19 (15), 2568–2580. [PubMed: 31243422]

61. Guo Y Sensitive, label-free biomolecular binding detection using a one-dimensional photonic crystal sensor. University of Michigan, 2010.
62. Scudder J Optimization of the limulus amoebocyte lysate test via use of a photonic crystal biosensor. The University of Texas at San Antonio, 2016.
63. Trabucco L; Gonzalez C; Ridoutt A; Kishwar A; Chaj-Ulloa J; Attia M; Yazdani N; Akimov N; Ye JY In Functionalization of a photonic crystal biosensor with modified aptamers for the detection of cardiac biomarkers, Label-free Biomedical Imaging and Sensing (LBIS) 2022, SPIE: 2022; pp 99–106.
64. Lim ZW; Varma VB; Ramanujan RV; Miserez A, Acta Biomaterialia 2020, 110, 221–230. [PubMed: 32422317]
65. Ramirez T; Strigun A; Verlohner A; Huener H-A; Peter E; Herold M; Bordag N; Mellert W; Walk T; Spitzer M, Archives of toxicology 2018, 92, 893–906. [PubMed: 28965233]
66. Chen Z; Long L; Wang J; Li W; Wang A; Kankala RK; Zou L; Liu Y, ACS omega 2024.
67. Ramaiahgari SC; Den Braver MW; Herpers B; Terpstra V; Commandeur JN; van de Water B; Price LS, Archives of toxicology 2014, 88, 1083–1095. [PubMed: 24599296]
68. Li R; Liu F; Chang Y; Ma X; Li M; Li C; Shi C; He J; Li Y; Li Z, Toxicology mechanisms and methods 2017, 27 (6), 401–407. [PubMed: 28412881]
69. Anadón A; Castellano V; Martínez-Larrañaga MR, Biomarkers of drug toxicity. In Biomarkers in toxicology, Elsevier: 2014; pp 593–607.
70. Ozer JS; Chetty R; Kenna G; Koppiker N; Karamjeet P; Li D; Palandra J; Lanevschi A; Souberbielle BE; Ramaiah S, Biomarkers in Medicine 2010, 4 (3), 475–483. [PubMed: 20550481]
71. Akimov N; Scudder J; Ye JY, Biosensors and Bioelectronics 2021, 191, 113436. DOI 10.1016/j.bios.2021.113436. [PubMed: 34157598]
72. Guo Y; Ye JY; Divin C; Huang B; Thomas TP; Baker JJR; Norris TB, Analytical Chemistry 2010, 82 (12), 5211–5218. DOI 10.1021/ac100576y. [PubMed: 20486666]
73. Peterson R; Solis S; Zhang B; Huang H; Ye JY, Opt Lett 2013, 38 (15), 2739–41. DOI 10.1364/OL.38.002739. [PubMed: 23903128]
74. Ye JY; Gestwicki J; Norris TB; Baker J, J R; Bersono-Begey T, Patent No. 8,497,992.
75. De Picciotto S; Imperiali B; Griffith LG; Wittrup KD, Analytical biochemistry 2014, 460, 9–15. [PubMed: 24814226]

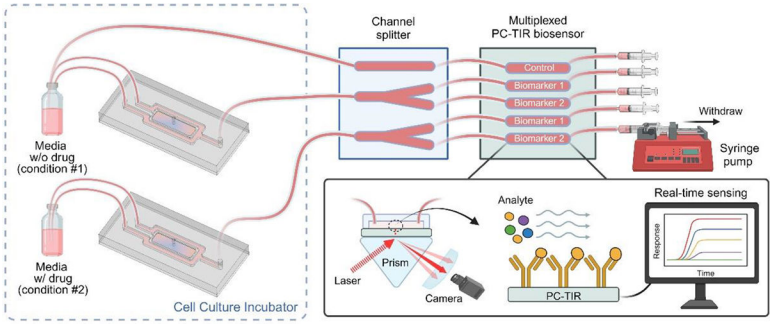

Figure 1. Integration of a 3D liver on-a-chip with a PC-TIR optical biosensor for rapid, continuous, and multiplexed monitoring of liver-secreted biomarkers.

The integrated microfluidic-based system comprises a 3D liver on-a-chip model connected to a microchannel splitter chip and a PC-TIR biosensor that detects protein biomarkers in solution. This configuration allows the rapid and continuous monitoring of liver-secreted biomarkers to detect drug-induced toxicity in organ on-a-chip models rapidly. Figure created with BioRender.com.

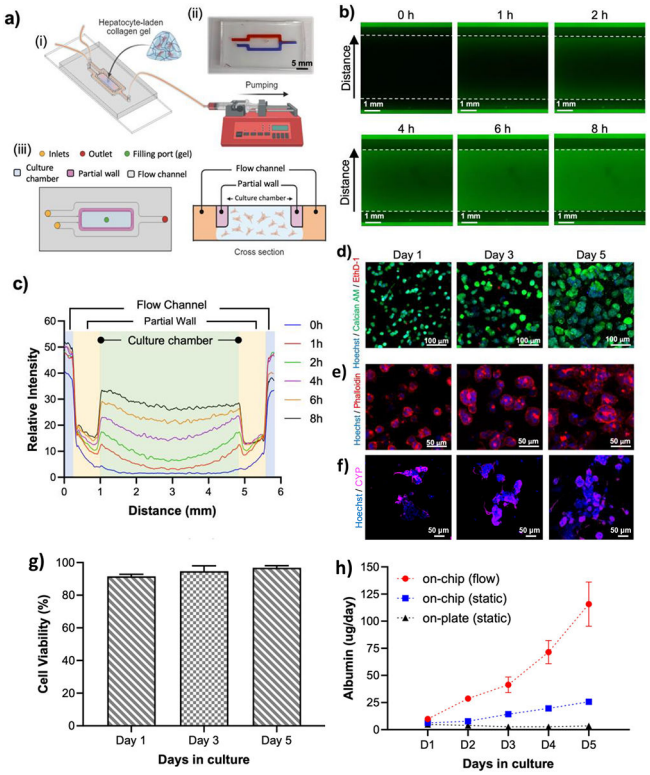

Figure 2. Validation of the 3D liver on-a-chip model.

(a) Schematic of the collagen-based 3D liver on-a-chip platform: (i) The HepG2-laden collagen hydrogel is loaded into the central cell culture chamber of the liver chip and perfused by withdrawing cell culture media from the outlet port using a syringe pump; (ii) Picture of an actual chip with food die in its side channels; and (iii) top and cross-sectional views of the 3D liver on-a-chip model. Figure created with BioRender.com. **(b)** Fluorescence images of FITC-Dextran diffusion in the collagen-loaded cell culture chamber from 0 to 8 hours. **(c)** Relative FITC intensity distribution within the collagen-loaded cell culture chamber of the 3D liver on-a-chip from 0 to 8 hours. **(d)** Fluorescent staining of live (green), dead (red), and nucleus (blue) showing the viability of HepG2 cells after 1, 3, and 5 days of dynamic culture on-chip. **(e)** Fluorescent staining of the cytoskeleton (red) and nucleus (blue) showing cell growth and clustering in the collagen hydrogel. **(f)** Immunofluorescence staining of CYP (purple) with nuclear counterstain by Hoechst (blue). **(g)** Cell viability of HepG2 cells after 1, 3, and 5 days of dynamic culture on-chip. **(h)** Daily albumin secretion from HepG2 cells cultured on-chip under dynamic flow and static conditions and off-chip (96-well plate) for 5 days.

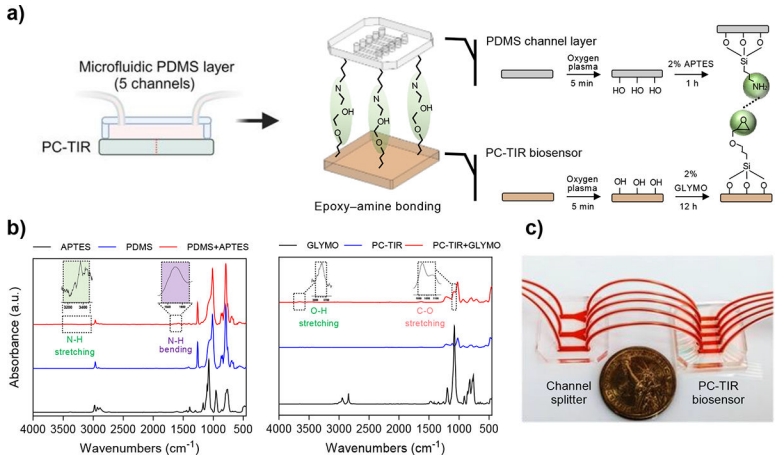

Figure 3. Fabrication of the compact portable microfluidics-integrated PC-TIR biosensor.

(a) Assembly protocol of the multiplexed PC-TIR biosensor using an epoxy-amine reaction to bond a PDMS microchannel layer to the PC-TIR biosensor. Figure created with BioRender.com. **(b)** FTIR spectroscopy analysis of the epoxy-modified PC-TIR biosensor and the amine-modified PDMS. **(c)** Photograph of the assembled PC-TIR biosensor connected to a channel splitter to control liquid routing.

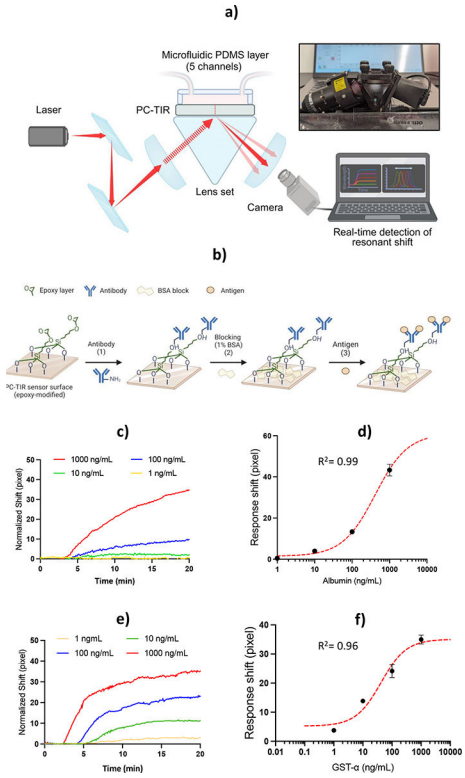

Figure 4. Performance evaluation of PC-TIR biosensors for biomarker detection.

(**a**) Schematic of the PC-TIR device comprising a PC-TIR biosensor, a microfluidic PDMS layer, and a portable optical setup that includes a diode laser, lens assembly, a CMOS camera, and custom software. Inset: Photograph of the assembled PC-TIR device. (**b**) Schematic showing the functionalization process of the PC-TIR biosensor for biomarker detection. (**c)** Kinetic response curves showing antibody-antigen binding at different concentrations of human albumin and (**d**) its calibration curve according to the equilibrium shift of exponential nonlinear regression. (**e**) Kinetic response curves showing antibody-antigen binding at different concentrations of human GST-α and (**f**) its calibration curve according to the equilibrium shift of exponential nonlinear regression. (**a** and **b**) was created with BioRender.com.

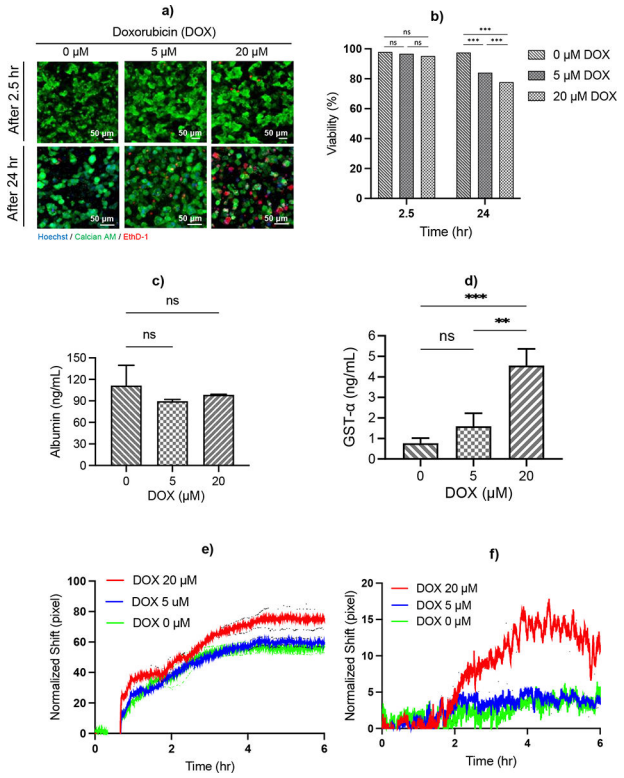

Figure 5. Real-time detection of DOX-induced toxicity using the integrated system of a liver-on-a-chip with a PC-TIR biosensor.

(**a**) Live/dead staining of the HepG2 cells in the 3D liver on-a-chip model after treatment with 0, 5, and 20 μM DOX for 24 h. (**b**) Cell viability of the HepG2 cells in the 3D liver on-a-chip model after treatment with 0, 5, and 20 μM DOX for 2.5 h and 24 h. (**c**) Secretion level of albumin from the 3D liver-on-a-chip after 24 h treatment. (**d**) Secretion level of GST-α from the 3D liver on-a-chip after 24 h treatment. (**e**) In-line rapid and continuous measurements of albumin secreted from the 3D liver on-a-chip. (**f**) In-line rapid and continuous measurements of GST-α secreted from the 3D liver on-a-chip.